ELSEVIER

Journal of Power Sources 75 (1998) 244–250

JOURNAL OF POWER SOURCES

Preparation and characteristics of $(Na_yAg_{1-y})_2V_4O_{11}$ for lithium secondary battery cathodes

Jin Kawakita *, Koji Makino, Yasushi Katayama, Takashi Miura, Tomiya Kishi

Department of Applied Chemistry, Faculty of Science and Technology, Keio University, Hiyoshi 3-14-1, Kohoku-ku, Yokohama, 223-8522, Japan

Received 15 May 1998; accepted 1 June 1998

Abstract

Layered vanadium oxides, $(Na_yAg_{1-y})_2V_4O_{11}$ ($y = 0.77–0.98$) are prepared by substituting part of the silver ions in $Ag_2V_4O_{11}$ with sodium ions using an ion-exchange reaction in molten nitrate salts. These oxides exhibit less capacity loss during repeated cycling than non-substituted oxide, $Ag_2V_4O_{11}$. This is mainly because the structural change into an amorphous state upon lithiation is restricted by the pillar effect in which unextractable sodium ions connect adjacent layers during lithium insertion/extraction. © 1998 Elsevier Science S.A. All rights reserved.

Keywords: Silver vanadate; Sodium; Ion exchange; Lithium; Discharge capacity

1. Introduction

Silver vanadium oxide (SVO) with the formula $Ag_2V_4O_{11}$ or $AgV_2O_{5.5}$ has been successfully used as the positive electrode for a primary lithium battery [1–5]. Both the shape of the discharge curve and the high-rate capability of the Li/SVO system make it ideal as a power source for implantable cardiac defibrillators. As SVO has a stepped discharge curve, the state of discharge of the battery can be estimated by measuring the battery potential. This feature is desirable in an implanted medical device. Other advantages of SVO are: (i) conductive material, such as carbon black, is not required because metallic silver formed during the early stages of discharge increases the total conductivity of the cathode; (ii) it is possible to discharge with a large pulse current on a trace background current.

The cell parameters of the stoichiometric compound, $Ag_2V_4O_{11}$, and the oxygen-deficient phase, $Ag_2V_4O_{11-y}$ have been reported [6,7]. Zandbergen et al. [8] disclosed that there is quite a small content of metallic silver in the resulting material when the formula is $Ag_{2-x}V_4O_{11}$ ($x = 0.078$ when synthesized using Ag_2O and V_2O_5 in a molar ratio of 1:2). They also determined two types of structure for $Ag_{2-x}V_4O_{11}$ using high resolution electron microscopy, and the stacking of V_4O_{11} layers in the *c*-axis direction.

Many authors [9–13] have investigated the lithium insertion behaviour of $Ag_2V_4O_{11}$ including the non-stoichiometric silver vanadium oxide mentioned above. Crespi et al. [13] reported that although the V_4O_{11} layers were retained, there was random stacking of the layers during lithium insertion. In the early stages of discharge, metallic silver was deposited by reduction of $Ag_2V_4O_{11}$ [11].

It was reported [14,15] that the lithium intercalation process is reversible with respect to the crystal structure and the composition-potential profile. This finding was drawn from the results of discharge and charge tests of $Ag_2V_4O_{11}$. On the other hand, long-term cycling through the silver reduction/oxidation region leads to a fast decline in capacity, probably influenced by the volume changes associated with the formation/annihilation of metallic silver particles [15].

To minimize the capacity loss, it is aimed to connect the adjacent V_4O_{11} layers with cations which do not possess redox activity. In this paper, a report is given of the preparation of $(Na_yAg_{1-y})_2V_4O_{11}$ by substitution of part of the Ag^+ ions with Na^+ ions between the V_4O_{11} layers. Data from discharge–charge cycling tests of these vanadium oxides are also presented.

* Corresponding author. Tel.: +81-45-563-11-41; Fax: +81-45-563-59-67; E-mail: kawakita@chem. keio.ac.jp

0378-7753/98/$19.00 © 1998 Elsevier Science S.A. All rights reserved.
PII: S0378-7753(98)00118-9

2. Experimental

Silver vanadium oxide ($Ag_2V_4O_{11}$) was prepared via a solid-state reaction of Ag_2O (Tokuriki Chemical, 99.0% purity) and V_2O_5 (Soekawa Chemical, 99.5% purity), as described by Zandbergen et al. [8]. These two reagents were mixed, in an appropriate ratio, in an agate mortal and pestle, and then pressed at 2×10^6 g cm^{-2} to form a pellet (20 mm diameter $\times$ 1 mm height). This pellet was heated at 500°C under an oxygen atmosphere for 6 h. The resulting oxide was sieved under 38 μm. The ion-exchange reaction was carried out by dispersing the sample powder in molten nitrate salt ($NaNO_3$, 99.0% purity, Kanto Chemical; and $AgNO_3$, > 99.8% purity, Wako Chemical) in an aluminum crucible in air. The following experimental conditions were varied (Table 1): temperature, reaction time, composition of the molten salt, ratio of molten salt to sample, and repetition number.

The resulting mixtures were washed with ion-exchanged water and filtered to separate the desired oxide from the mixture. Then, the products were heated at 60°C, followed by 90°C, for 24 h. The samples were characterized in terms of their crystal structure by means of powder X-ray diffraction (XRD) analysis (using Rigaku apparatus, RINT-1300, Cu K_α radiation with a nickel filter). The chemical composition was determined by elemental analysis using atomic absorption for silver and vanadium, and flame emission spectroscopy for sodium (Hitachi, 180-55 AAS).

The procedure used for electrochemical measurements has been reported elsewhere [16]. A cylindrical glass cell was used. This housed the three electrodes at 25°C. Metallic lithium wires (Aldrich, 3.2 mm diameter) served as the counter and reference electrodes. The working electrode was prepared by mixing the powdered oxide, acetylene black (Denka Black, Denki Kagakukogyo), and poly(tetrafluoroethylene) (PTFE, Mitsui-Du Pont) in a weight ratio of 70:25:5. The resulting sample was formed into a pellet (0.5 mm diameter) by pressing on to a porous nickel net at 2×10^6 g cm^{-2}. All of the pellet, except for the surface, was insulated with silicone resin (Shinetsu Silicone, KE-450). One side of the pellet had a surface area of 0.196 cm^2 and the opposite side was connected to a copper lead with gold paste (Tokuriki Chemical, P-248). The electrolyte was a 1 M solution of lithium perchlorate ($LiClO_4$) in a propylene carbonate (PC) solution (Mitsubishi Chemical, water content < 20 ppm). Electrochemical measurements were performed with a potentiostat (Toho Technical Research, PS-08) which was controlled by a personal computer (NEC, PC-9801). Discharge–charge tests were carried out under galvanostatic conditions at a current density of ±50 to 300 μA cm^{-2}. The amount of inserted lithium was calculated from the quantity of electricity passed through the working electrode. The potential was taken as the quasi open-circuit potential (OCP) when the change in the open-circuit potential was within 1 mV h^{-1} after a discharge or a charge experiment. An XRD measurement was performed after each electrochemical experiment. The sample was placed in an aluminum sample holder after removing the silicone resin and the copper lead and thorough washing with PC solvent. The opposite side of the window of this aluminum holder was covered with a glass plate. The sample was fixed on clay in the centre of the glass plate to maintain a constant position during XRD analysis.

3. Results and discussion

3.1. Preparation of $(Na_y Ag_{1-y})_2V_4O_{11}$

Various silver vanadium oxides such as $Ag_4V_2O_7$, β-$Ag_{0.33}V_2O_5$ and δ-$Ag_{0.68}V_2O_5$ are formed at a reaction temperature above 350°C and at a higher molar ratio of $AgNO_3$ to $Ag_2V_4O_{11}$, regardless of the composition of the molten salt ($AgNO_3$ and $NaNO_3$). Therefore, an ion-exchange reaction which involves replacement of part of the Ag^+ ions with Na^+ ions between V_4O_{11} layers occurs only in pure molten $NaNO_3$ medium.

Fig. 1 shows the relation between the reaction time and y in $(Na_yAg_{1-y})_2V_4O_{11}$. The latter was prepared by an ion-exchange reaction of Ag^+ ions in $Ag_2V_4O_{11}$ with Na^+ ions at 350°C in molten $NaNO_3$, where the molar ratio of $Ag_2V_4O_{11}/NaNO_3$ was 1/100. As the reaction proceeded, the content of sodium increased rapidly and approached almost a constant value beyond 18 h. In this experiment, therefore, the ion-exchange reaction reaches an equilibrium state at about 24 h.

Table 1
Experimental conditions of ion-exchange reaction

Temperatures (°C)	Reaction time (h)	Molar ratio of molten salt to oxide	Molar ratio[a] of Na to Ag of molten salt	Repeat number
350	24	100	0 to 1.0	1
320 to 400	24	100	1.0	1
350	0.33 to 30	100	1.0	1
350	24	40 to 600	1.0	1
350	24	100	1.0	1 to 5

[a]Ratio corresponds to initial composition of molten salt composed of $NaNO_3$ and $AgNO_3$.

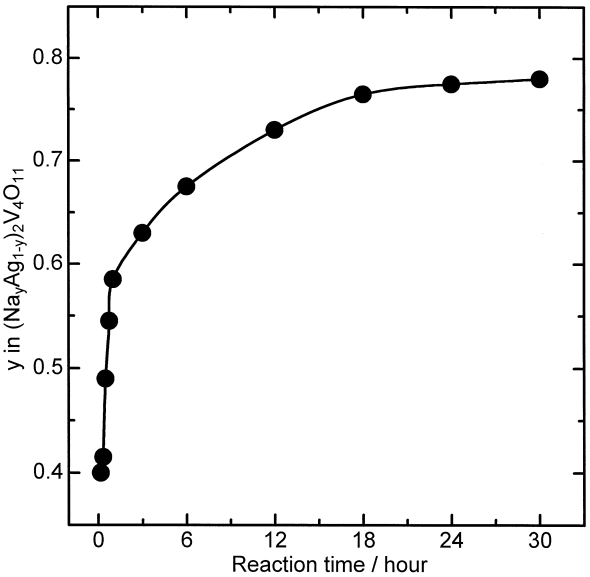

Fig. 1. Relation between reaction time and y in $(Na_yAg_{1-y})_2V_4O_{11}$, ($Ag_2V_4O_{11}$ / $NaNO_3$ = 1/100 at 350°C).

Fig. 2 presents XRD patterns of $(Na_yAg_{1-y})_2V_4O_{11}$ prepared by substituting part of the Ag^+ ions with Na^+ ions between the layers. All the peaks of the starting material (sodium content, $y = 0$) were indexed to the monoclinic system (space group: $C2/m$, $a = 15.29$ Å, $b = 3.58$ Å, $c = 9.50$ Å, and $\beta = 127.78°$), as shown in Fig. 2(a). Beyond $y = 0$, additional peaks appear. These cannot be ascribed to $Ag_2V_4O_{11}$. By way of example, the XRD pattern for $y = 0.68$ is given in Fig. 2(b). For $0.77 < y < 0.98$, the peaks associated with $Ag_2V_4O_{11}$ disappear, as demonstrated by the pattern for $y = 0.77$ (Fig. 2(c)). This phenomenon is confirmed by the fact that when the relative intensity of the (001) line ascribed to $Ag_2V_4O_{11}$ phase is plotted versus the y value, it becomes zero at about $y = 0.8$ on extrapolation of the straight line approximated by the least squares rule. The new diffraction pattern can be interpreted as follows: silver ions with a large X-ray scattering factor are exchanged by sodium ions and cause an increase in the relative intensity of (001) diffraction line. If the line near 12° in 2θ is assigned to the (001) diffraction line of the new phase, the diffraction lines ascribed to other $(00l)$ planes ($l = 2$ and 3) appear exactly in the expected angles in 2θ as, for example, in the pattern for $y = 0.77$ (Fig. 2(c)). Presumably, these results indicate the formation of a Na-rich oxide, $(Na_yAg_{1-y})_2V_4O_{11}$, with a layered structure analogous to that of $Ag_2V_4O_{11}$, by substitution of part of the Ag^+ ions with Na^+ ions between the layers. The XRD pattern for $y = 0.77$ is almost the same as that for $y = 0.93$, (cf., Fig. 2(c) and (d)), despite the fact that the two patterns have a slight difference in the position (2θ) and the relative intensity of some diffraction lines that are mainly due to substitution of silver with sodium. Accordingly, XRD measurements show that the ion-exchange proceeds as a single-phase reaction in the region of $0.77 < y < 0.98$.

The relation between y in $(Na_yAg_{1-y})_2V_4O_{11}$ and the mol fraction of sodium in the molten salt in equilibrium (= Na/(Na + Ag) at final state) is shown in Fig. 3. For mol fraction of sodium smaller than 0.980, silver-rich vanadium oxides such as $Ag_4V_2O_7$ are obtained as products not by the ion-exchange reaction but by the reaction of $Ag_2V_4O_{11}$ with $AgNO_3$. This phenomenon can be explained by examining the phase diagram of the V_2O_5–

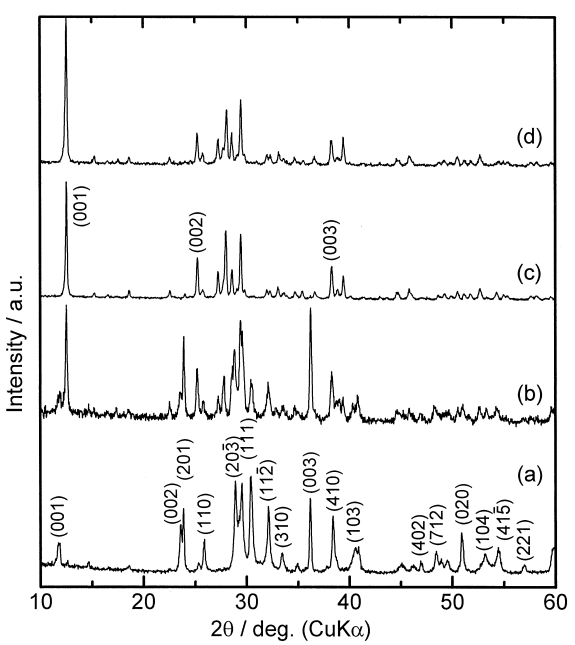

Fig. 2. XRD patterns of $(Na_yAg_{1-y})_2V_4O_{11}$, (a: $y = 0$, b: $y = 0.68$, c: $y = 0.77$, and d: $y = 0.93$).

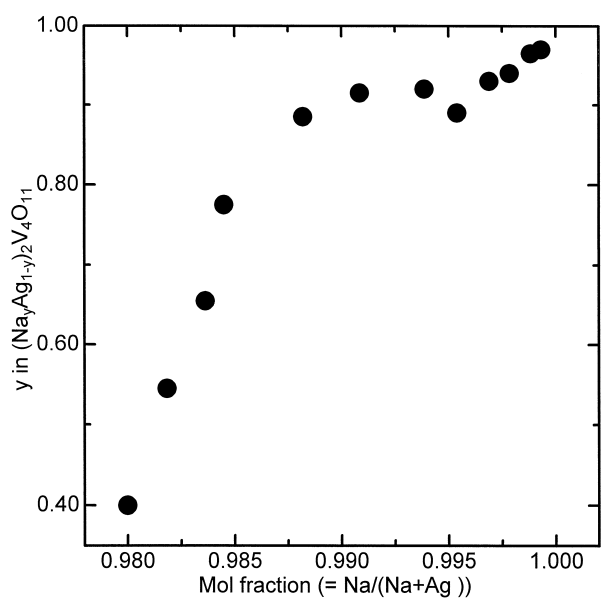

Fig. 3. Relation between y in $(Na_yAg_{1-y})_2V_4O_{11}$ and mol fraction of sodium (= Na/(Na + Ag)) in molten salt in equilibrium (reaction time: 24 h).

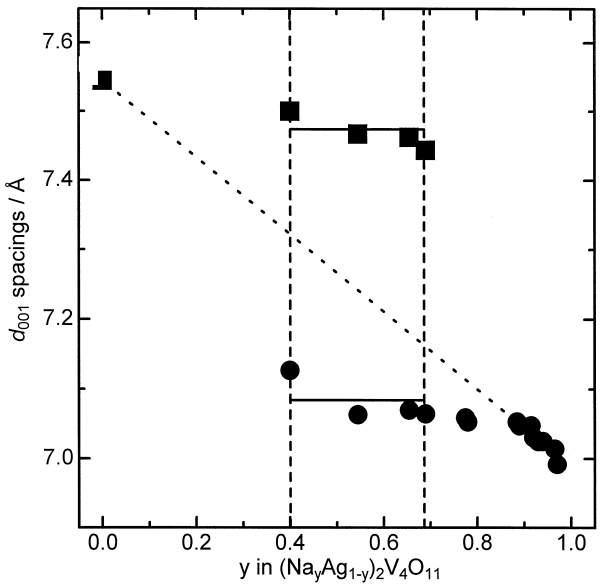

Fig. 4. Relation between d_{001} spacings and y in $(Na_yAg_{1-y})_2V_4O_{11}$, (■: $Ag_2V_4O_{11}$ phase and ●: $(Na_yAg_{1-y})_2V_4O_{11}$ phase).

Ag_2O system [17]. When the fraction in the molten salt is beyond 0.980 ($y > 0.40$), the silver vanadates (described above) disappear. Nevertheless, two phases ascribed to $Ag_2V_4O_{11}$ and $Na_2V_4O_{11}$ type oxides are observed for $0.40 < y < 0.77$, as mentioned in the interpretation of the XRD pattern (see Fig. 2(b)). At $0.77 < y < 0.9$, only the second phase exists. Two types of a second phase with $y \approx 0.9$ and with different crystal structures might exist, as there is more or less a constant composition region with respect to the y value thought the mol fraction of sodium in the molten salt increases. At $y > 0.90$, a linear relationship is observed between the mol fraction and the y value.

The relationship between the d_{001} spacing calculated from the XRD pattern and y in $(Na_yAg_{1-y})_2V_4O_{11}$ is presented in Fig. 4. It has been reported [8] that the V_4O_{11} layers are stacked in the direction of the *c*-axis. Thus, the d_{001} spacing corresponds to the interlayer distance. In the two-phase region of $0.40 < y < 0.77$, the almost constant large and small spacings are attributed to $Ag_2V_4O_{11}$ and $Na_2V_4O_{11}$ type oxides, respectively. This result is explained by the fact that the ionic radus of sodium (r_{Na^+} = 1.16 Å [18]) is smaller than that of silver (r_{Ag^+} = 1.29 Å, octahedral coordination [18]). In the region where the $Ag_2V_4O_{11}$ phase disappears, the constant d_{001} spacing ($0.77 < y < 0.9$) and the subsequent linear decrease in d_{001} spacing ($0.9 < y < 1.0$) can correspond to the dependence of y on the mol fraction of the molten salt (see Fig. 3), and the region can be regarded as the 'ideal' single-phase. On the other hand, the structural and equilibrium behaviour of the region at $0.77 < y < 0.9$ is not well understood, and the crystal structure of the Na-substituted vanadate requires detailed investigation. In Section 3.2, electrochemical measurements are carried out on the sample ($y = 0.77$) determined as the single phase from XRD analysis.

3.2. Discharge characteristics of $(Na_yAg_{1-y})_2V_4O_{11}$

Discharge curves of $(Na_yAg_{1-y})_2V_4O_{11}$ at -50 μA cm^{-2} are shown in Fig. 5. The shape and capacity of the non-substituted oxide ($y = 0$) are in good agreement with those reported by other researchers [14,15]. While the total capacity of Na-substituted oxide ($y = 0.77$) is smaller than that of the oxide ($y = 0$) by about $\Delta x = 2.0$, the potentials at which the plateau and inflection appear are similar for both oxides. This phenomenon reflects the structural similarity between $Ag_2V_4O_{11}$ and Na-substituted oxide, described above. The discharge curves can be divided into four domains, I to IV. XRD patterns of lithiated $Ag_2v_4O_{11}$ ($y = 0$) and $Na_{1.54}Ag_{0.46}V_4O_{11}$ ($y = 0.77$) are given in Fig. 6. In the early discharged state ($x = 0.5$) of both oxides, Ag^1 is reduced and substituted with inserted Li^+ ions. Accordingly, deposited metallic silver is observed in addition to the original phase, as shown in Fig. 6(a) and (c). As well as $Ag_2V_4O_{11}$ reported by other authors [11], this phenomenon was observed with $Ag_{1+x}V_3O_8$ [19] and δ-$Ag_yV_2O_5$ [20]. When deeply discharged up to 2.0 V (versus Li), the XRD pattern of the lithiated oxide up to $x = 6.0$ for $Ag_2V_4O_{11}$ ($y = 0$) indicates that the structure becomes amorphous, as seen as in Fig. 6(b). On the other hand, the Na-substituted oxide ($y = 0.77$) still has the two peaks ascribed to the starting material irrespective of the x value, as shown in Fig. 6(d) (marked by arrows). When Li^+ ions are inserted in the early stages of discharge, the interlayer spacing of the lithiated compound for $(Na_yAg_{1-y})_2V_4O_{11}$ decreases, as shown in Fig. 7. This

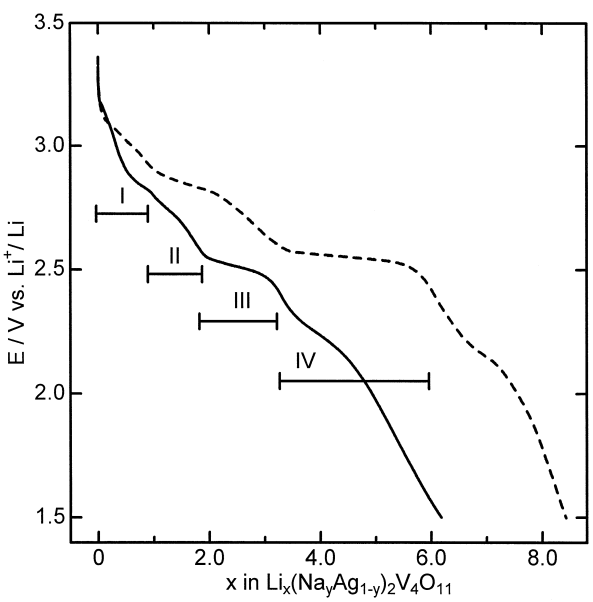

Fig. 5. Discharge curves of $(Na_yAg_{1-y})_2V_4O_{11}$ at -50 μA cm^{-2} (dashed line, $y = 0$; solid line, $y = 0.77$).

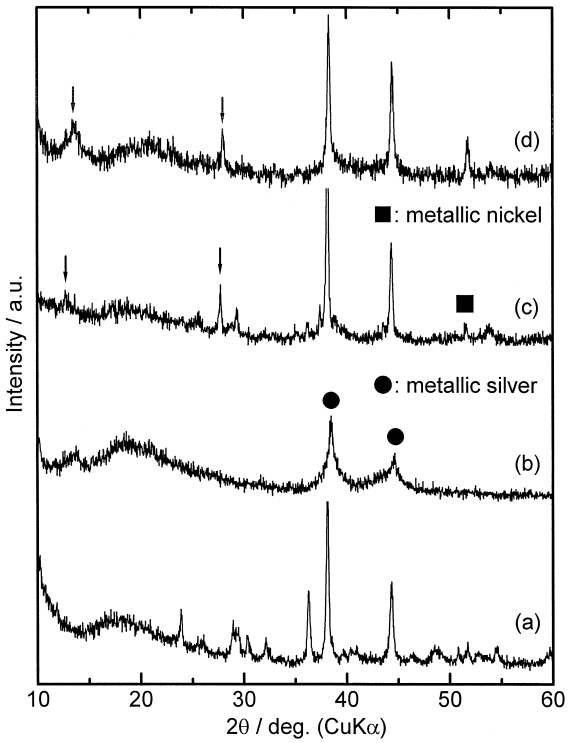

Fig. 6. XRD patterns of lithiated $Ag_2V_4O_{11}$ ($y = 0$; a: $x = 0.5$ and b: $x = 6.0$), and lithiated $Na_{1.54}Ag_{0.46}V_4O_{11}$ ($y = 0.77$; a: $x = 0.5$ and b: $x = 4.5$).

phenomenon was also reported for $Ag_2V_4O_{11}$ by Leising et al. [11]. The two-phase region begins at different x values between $y = 0$ and $y = 0.77$. Presumably, this is caused by the small number of silver ions required to maintain the original host structure.

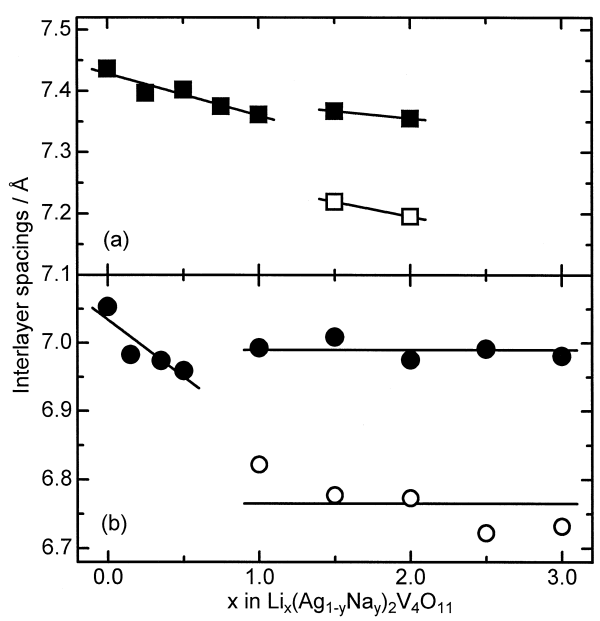

Fig. 7. Relation between interlayer spacing and x in $Li_x(Na_yAg_{1-y})_2V_4O_{11}$ (a: $y = 0$, and b: $y = 0.77$).

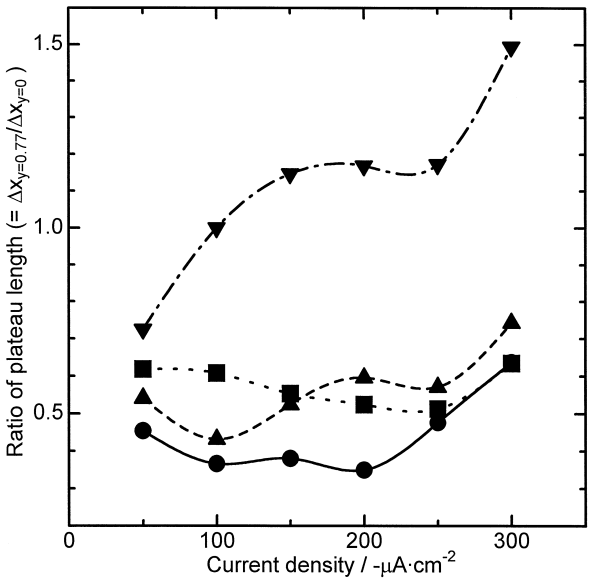

Fig. 8. Dependence of ratio of plateau length ($= \Delta x_{y=0.77}/\Delta x_{y=0}$) on current density during discharge (●: 1st, ▲: 2nd, ■: 3nd, and ▼: 4th plateau).

Fig. 8 shows the dependence of the ratio of the lengths (Δx: the amount of inserted Li^+ ions) of the I to IV domains on the current density during discharge. The ratio represents $\Delta x_{y=0.77}/\Delta x_{y=0}$. Except for domain IV, the ratios are less than unity in the current density range -50 to 300 μA cm^{-2}. Probably, this decrease in the three domain lengths corresponds to a decrease in the number of electron acceptable Ag^I ions by substitution with Na^+ ions. Thus, it is considered that the simultaneous reduction of Ag^I and V^V occurs even on the third step. By contrast, the ratio for the fourth plateau increases above 1.0 beyond a current density of -100 μA cm^{-2}. This result indicates that the pronounced effect of Na^+ ions on restraining the change in the crystal structure to an amorphous state appears during the fourth domain where reduction of the vanadium component occurs dominantly.

3.3. Cycling behaviour of $(Na_yAg_{1-y})_2V_4O_{11}$

The initial discharge and charge cycle curves of $(Na_yAg_{1-y})_2V_4O_{11}$ at ± 50 μA cm^{-2} are shown in Fig. 9; the cut-off potential is 2.65, 2.5 or 1.5 V. A small capacity loss is observed on the first cycle up to the second domain. According to the investigation by West and Crespi [15], metallic silver formed during discharge is oxidized and re-enters the host structure during charging. This process is indicated by the potential plateau near 3.5 V because the length of this plateau is smaller in the Na-substituted oxide than in the original silver-rich oxide. By contrast, domains I and II do not appear clearly on the charging curves. This behaviour can be explained by the assumption that re-entering of Ag^+ ions into the structure is slower than extraction once silver atoms are aggregated and deposited as

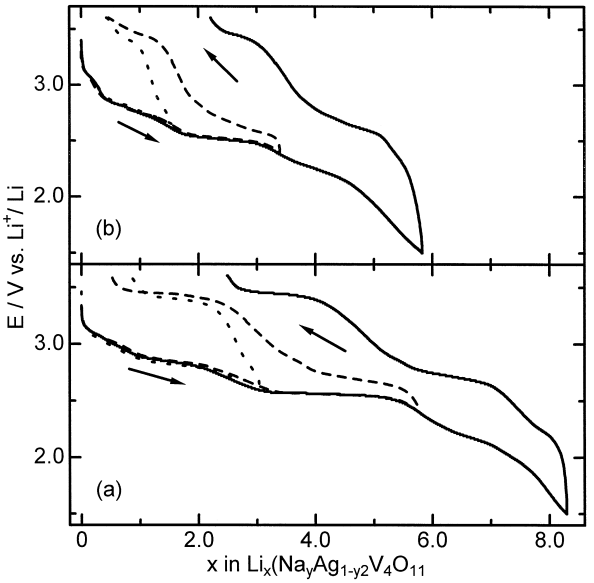

Fig. 9. First discharge and charge cycle curves of $(Na_yAg_{1-y})_2V_4O_{11}$ at ± 50 μA cm^{-2} with cut-off potential of 2.65, 2.5 or 1.5 V (a: $y = 0$, and b: $y = 0.77$).

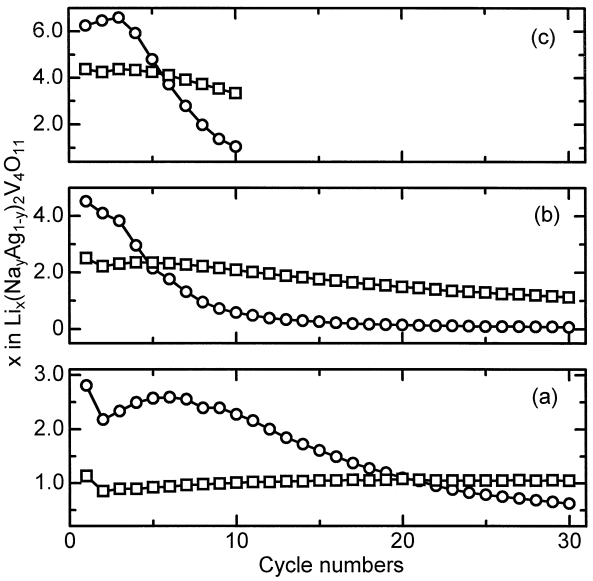

Fig. 11. Relation between cycle number and x in $Li_x(Na_yAg_{1-y})_2V_4O_{11}$ at ± 200 μA cm^{-2} with cut-off potential of (a) 2.6, (b) 2.45 and (c) 1.5 V (○: $y = 0$, and □: $y = 0.77$).

metallic particles; an assumption supported by the large polarization between discharge and charge curves. On the other hand, large capacity losses are observed on the charging curves of both oxides after deep discharge up to 1.5 V. These losses are probably due to the irreversibility of the lithium insertion/extraction process in the fourth domain rather than to the formation/annihilation of silver particles.

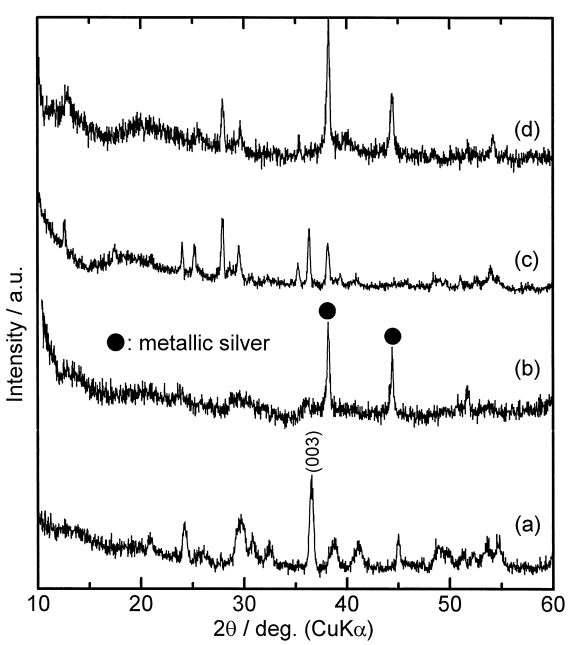

Fig. 10. XRD patterns of $(Na_yAg_{1-y})_2V_4O_{11}$: (a) starting material of $y = 0$; (b) after 1st cycle of $y = 0$ at 1.5 V cut-off; (c) as starting material of $y = 0.77$; (d) after 1st cycle of $y = 0.77$ at 1.5 V cut-off.

After the first discharge/charge cycle, both oxides exhibit similar XRD patterns, regardless of the cut-off potential, see Fig. 10(b) and (d). The Na-substituted oxide ($y = 0.77$), however, displays a pattern with more sharp and strong diffraction lines except for the lines ascribed to the remaining metallic silver, compared with the non-substituted oxide, $Ag_2V_4O_{11}$. This observation may support the idea that unextractable Na^+ ions combine in the adjacent layers and such a pillar effect can inhibit the change in the structure to the amorphous state.

Fig. 11 presents the relation between cycle number and discharge capacity, x in $Li_x(Ba_yAg_{1-y})_2V_4O_{11}$ at ± 200 μA cm^{-2} with a cut-off potential of 2.6, 2.45 or 1.5 V. The decrease of discharge capacity with the cycle number is marked for the oxide with $y = 0$, though the capacity during the earlier stages of cycling is larger than that for the Na-substituted oxide. These properties are caused by: (i) the contribution of Ag^I to the insertion reaction: (ii) the slow rate of extraction/insertion; (iii) amorphization of the crystal. The constant capacity of the oxide with $y = 0.77$, may be due to the pillar effect of Na^+ ions in the interlayer, especially under deep discharge conditions up to 1.5 V.

4. Conclusions

Layered vanadium oxides, $(Na_yAg_{1-y})_2V_4O_{11}$ ($y = 0.77$–0.98), are prepared by substituting part of the silver ions in $Ag_2V_4O_{11}$ with sodium ions using an ion-exchange reaction in molten $NaNO_3$. The oxides have a smaller interlayer spacing with less Na^+ ions between the layers.

The discharge curve at a current density of 50 to 300 $\mu A\ cm^{-2}$ has plateaux in the stepwise potential change, which divide the extent of lithium insertion into four domains. Reduction of Ag^{I} continues to occur up to the third domain in competition with reduction of V^{V}, and thus the extent of these three domains is smaller in the case of Na-substituted oxide ($y = 0.77$). The extent of lithium insertion during the fourth domain is larger, however, because of the pillar effect in which unextractable sodium ions continue to connect the adjacent layers and restrict change of the structure into an amorphous state upon lithiation.

The oxide with $y = 0.77$ shows less capacity loss during repeated cycling compared with the non-substituted oxide, $Ag_2V_4O_{11}$, mainly because the pillar effect is maintained during lithium insertion/extraction.

References

[1] G.M. Bergman, S.J. Ebel, E.S. Takeuchi, P. Keister, J. Power Sources 20 (1987) 179.
[2] E.S. Takeuchi, P. Keister, J. Power Sources 21 (1987) 13.
[3] G.M. Bergman, E.S. Takeuchi, J. Power Sources 26 (1989) 365.
[4] A.M. Crespi, P.M. Skarstad, J. Power Sources 43/44 (1993) 119.
[5] E.S. Takeuchi, J. Power Sources 54 (1995) 115.
[6] R.P. Ozerov, Zh. Neorg. Khim. 4 (1959) 1047.
[7] B. Raveau, Rev. Chim. Minér. 4 (1967) 729.
[8] H.W. Zandbergen, A.M. Crespi, P.M. Skarstad, J.F. Vente, J. Solid State Chem. 110 (1994) 167.
[9] E.S. Takeuchi, W.C. Thiebolt III, J. Electrochem. Soc. 135 (1988) 2691.
[10] E.S. Takeuchi, W.C. Thiebolt III, J. Electrochem. Soc. 138 (1991) L44.
[11] R.A. Leising, W.C. Thiebolt III, E.S. Takeuchi, Inorg. Chem. 33 (1994) 5733.
[12] R.A. Leising, W.C. Thiebolt III, Chem. Mater. 6 (1994) 489.
[13] A.M. Crespi, P.M. Skarstad, H.W. Zandbergen, J. Power Sources 54 (1995) 68.
[14] F. García-Alvarado, J.M. Tarascon, Solid State Ionics 73 (1994) 247.
[15] K. West, A.M. Crespi, J. Power Sources 54 (1995) 334.
[16] J. Kawakita, Y. Katayama, T. Miura, T. Kishi, Solid State Ionics 107 (1998) 145.
[17] P. Fleury, Rev. Chim. Minér. 6 (1969) 819.
[18] R.D. Shanon, Acta Crystallogr. A32 (1976) 751.
[19] J. Kawakita, Y. Katayama, T. Miura, T. Kishi, Solid State Ionics 99 (1997) 71.
[20] J. Kawakita, H. Sasaki, M. Eguchi, T. Miura, T. Kishi, J. Power Sources 70 (1998) 28.